Highly efficient transverse-electric-dominant ultraviolet-C emitters employing GaN multiple quantum disks in AlN nanowire matrix

Highly Efficient Transverse-Electric-Dominant Ultraviolet-C Emission Employing GaN Multiple Quantum Disks in AlN Nanowires Matrix

Ram Chandra Subedi,[1] Jung-Wook Min,[1] Somak mitra,[2] Kuang-Hui Li,[1] Idris Ajia,[2] Edgars Stegenburgs,[1] Dalaver H. Anjum,[3] Michele Conroy,[4] Kalani Moore,[4] Ursel Bangert,[4] Iman S. Roqan,[2] Tien Khee Ng,[1,*] Boon S. Ooi,[1,*]

[1]Photonics Laboratory, King Abdullah University of Science and Technology (KAUST), Thuwal 23955-6900, Kingdom of Saudi Arabia
[2]Semiconductor and Material Spectroscopy Laboratory, KAUST, Thuwal 23955-6900, Kingdom of Saudi Arabia;
[3]Imaging and Characterization Core Lab, KAUST, Thuwal 23955-6900, Kingdom of Saudi Arabia;
[4]Department of Physics and Energy, University of Limerick, Limerick V94 T9PX, Ireland

[*]tienkhee.ng@kaust.edu.sa , [*]boon.ooi@kaust.edu.sa

ABSTRACT

Heavy reliance on extensively studied AlGaN based light emitting diodes (LEDs) to replace environmentally hazardous mercury based ultraviolet (UV) lamps is inevitable. However, external quantum efficiency (EQE) for AlGaN based deep UV emitters remains poor. Dislocation induced nonradiative recombination centers and poor electron-hole wavefunction overlap due to the large polarization field induced quantum confined stark effect (QCSE) in "Al" rich AlGaN are some of the key factors responsible for poor EQE. In addition, the transverse electric polarized light is extremely suppressed in "Al"-rich AlGaN quantum wells (QWs) because of the undesired crossing over among the light hole (LH), heavy hole (HH) and crystal-field split-off (SH) states. Here, optical and structural integrities of dislocation-free ultrathin GaN quantum disk (QDisk) (~ 1.2 nm) embedded in AlN barrier (~ 3 nm) grown employing plasma-assisted molecular beam epitaxy (PAMBE) are investigated considering it as a novel nanostructure to realize highly efficient TE polarized deep UV emitters. The structural and chemical integrities of thus grown QDisks are investigated by high angle annular dark field scanning transmission electron microscopy (HAADF-STEM). We, particularly, emphasize the polarization dependent photoluminescence (PL) study of the GaN Disks to accomplish almost purely TE polarized UV (~ 260 nm) light. In addition, we observed significantly high internal quantum efficiency (IQE) of ~ 80 %, which is attributed to the enhanced overlap of the electron-hole wavefunction in extremely quantum confined ultrathin GaN QDisks, thereby presenting GaN QDisks embedded in AlN nanowires as a practical pathway towards the efficient deep UV emitters.

Keywords: Deep-ultraviolet emission, epitaxial growth, GaN quantum disks, transverse-electric-emission, quantum confinement

1. INTRODUCTION

In contrast to the conventional ultraviolet (UV) sources (mercury lamps), UV LEDs are compact, robust, environmentally friendly, exhibit long lifetimes, and well suited to various applications such as water/air purification, sterilization, medical treatment, memory devices, fluorescence-based biochemical sensing, military/defense purposes, and non-line-of-sight (NLOS) optical communication.[1–7] Particularly, with the invention of the gallium nitride (GaN) based blue light emitting diodes (LEDs),[8–10] lighting (indoor and outdoor) has shift its paradigm towards cleaner, sustainable, energy efficient and cost-effective source considering our dependency on nonrenewable fossil fuels and the environmental degradation form the usage of fossil fuels. Binary, ternary and quaternary combination of III-nitride material (In-Al-Ga-N) system covers a wide range of electromagnetic spectrum from deep ultraviolet (UV) to infrared (IR) spectrum.[11] Despite the vital breakthrough in the GaN material technology and transformation in the area of illumination, deep UV regime is

still at its infancy. Alloying AlN with GaN, Al-Ga-N based LEDs can be tuned to cover the spectral range (210 – 400 nm) changing the composition of Al. Despite the tunable nature of AlGaN, the excessive strain accumulation associated with increased alloying of Al in AlGaN[12] and the poor dopant activation due to the large ionization energy of the donors and acceptors are not favorable for realizing efficient deep-UV emitters.[13]. For the ternary compound bulk $Al_xGa_{1-x}N$ $\left(x \geq 0.25 \lambda \leq 315\text{nm}\right)$, the TE mode is severely suppressed by the TM mode, which is not favorable for vertical surface emitters. [14,15] The cut-off value of "x" for crossing over from TE to TM mode in $Al_xGa_{1-x}N$ also depends on the growth conditions and strain i.e. when $Al_xGa_{1-x}N$ is strained to AlN barriers, valance band crossover takes place for $x > 0.57$.[16] Hence, the likelihood of achieving highly efficient AlGaN-based deep-UV surface emitters is severely compromised if we simply employ an Al-rich AlGaN composition. While the exploration of a new material system is one of the possible ways to obtain highly efficient deep-UV devices,[17–20] developing a new material system and translating the system to an industrial application is non-trivial. Thus, employing novel nanostructures and nanofabrication techniques in an already well-developed technology is more likely to receive industrial adoption to accomplish highly efficient deep-UV emitters. Continuing along this path of using novel nanostructures, short superlattices (SLs) structures of AlN and GaN have been employed to realize TE dominant deep UV emitters, which have been summarized in Table 1. However, the experimental research regarding the investigation of optical polarization properties of such nanostructures in UV-C regime is still in the early state and hence further study in this regard is essential.

Table 1: Summary on the mid-deep UV emission using GaN/ AlN SLs structures

(Material), Structure	Emission Wavelength (nm)	TE – TM Quantification	Method	References
(GaN/ AlN), SLs	244	N/A	DFT calculation	Cui et *al.*[21]
(AlN/ GaN), SLs	224	N/A	First principle	Kamiya et *al.*[22]
(AlN/GaN), SLs based LED	276 – 237	N/A	Electrically pumped	Taniyansu et *al.*[23]
GaN/ AlN, SLs	224 – 255	N/A	Theoretical and experimental	Bayerl et *al.*[24]
(Al/GaN), SLs	236 – 312	N/A	Numerical analysis	Sun et *al.*[25]
(AlN/GaN), microdisk laser	275	N/A	Optically pumped	Selles et *al.*[26]
(AlN/GaN), QWs	249	TE dominant emission	Optically pumped	Shan et *al.*[27]
(GaN/AlN), delta	219	N/A	Optically pumped	Islam et *al.*[28]
(GaN/AlN), QWs	230 – 270	N/A	E-beam pumped	Wang et *al.*[29]
(GaN/AlN), delta	298	TE:TM ~ 15	Electrically pumped	Liu et *al.*[30]
(GaN/AlN), QDisks	250	N/A	Electrically pumped	Sarwar et *al.*[31]
(GaN/ AlN), QDisks	260 286	TE: TM ~ 361 TE:TM ~ 587	Optically pumped	Subedi et *al.*[32]

Most of the above listed research reports are based on planar structures and have not addressed the quantification of TE and TM modes except for few of the reports.[27,30,32] Planar device structures are not the most efficient nanostructures to unleash the full potential of the quantum confinement. Moreover, native substrates are very expensive, and growing planar nanostructure on highly mismatched foreign substrates leads to a high concentration of threading dislocations, generating nonradiative recombination centers and resulting in a poor IQE and hence low external quantum efficiency.[5,33] In contrast to the planar counterparts, nanowires (NWs) offer an excellent platform for the growth of the dislocation-free group III-N semiconducting materials on commercial scalable substrates.[34–37]

In this article, we report the growth of GaN QDisks embedded in the AlN NWs matrix using plasma-assisted molecular beam epitaxy (PA-MBE). We focus on the use of the ultrathin GaN QDisks without relying on the tuning of the conventional ternary AlGaN compound semiconductor for deep-UV emission. Additionally, we present a detailed structural characterization of GaN QDisks in AlN NWs followed by a thorough optical characterizations, i.e., temperature-dependent PL (TDPL), time-resolved PL (TRPL), and optical polarization measurements. More importantly, we quantify the TE and TM modes experimentally to realize TE-dominant PL emission in ultrathin GaN QDisks for efficient UVC emitters.

2. EXPERIMENTAL METHODS

GaN QDisks embedded in the AlN NWs matrix were grown on a 3-inch Si-substrate using a VEECO GEN 930 PAMBE system. Three samples that contains QDisks with different thicknesses were grown to elucidate the effect of quantum confinement: (a) Bulk (~ 20 nm) GaN, (b) 5-fold GaN QDisks, each with a thickness of ~ 3 nm separated by an AlN barrier of ~ 3 nm, and (c) 10-fold GaN QDisks, each with a thickness of ~ 1.2 nm separated by an AlN barrier of ~ 3 nm. Native oxide desorption in the MBE chamber is performed at 850 °C. GaN and seed layer was grown at 680 °C followed by the axial growth of the AlN barrier. The temperature was then increased to 750 °C for GaN QDisks followed by AlN capping. The Ga beam equivalent pressure (BEP) was fixed at 5×10^{-8} Torr, whereas the Al BEP was kept at 6 × 10–8 Torr. Nitrogen flow was maintained at 1.0 sccm with an RF power of 350 W. The detailed NW growth mechanism employing PA-MBE has been reported elsewhere.[38,39]

Time resolved PL (TRPL), measurements were carried out using the third harmonic line (250 nm) of a 750 nm ultrafast (150 fs) Ti:Sapphire laser (Coherent, Germany) converted by HarmoniXX THG unit (APE, Germany) as the laser excitation source. Pulse repetition rate of 2 MHz was obtained by a pulse picker unit (APE, Germany) where the laser spot diameter was kept at ~ 100 μm. The TDPL measurements were performed in the temperature window from 10 K to 290 K using a closed-cycle cryostat. Emission from the sample was detected using a SpectraPro 2300 spectrograph (using a grating with 150-gr/mm groove density) attached to a Hamamatsu C6860 streak camera with a temporal resolution of ~20 ps. The integration time was kept to 100 ms for 500 integrations. TRPL decay transients were fitted using a double exponential decay (equation 1):

$$Y = Y_o + A_{fast}e^{-t/t_{fast}} + A_{slow}e^{-t/t_{slow}} \quad (1)$$

where Y_o represents background signal, t_{fast} is the fast decay time, t_{slow} the slow decay time, and A_{fast} and A_{slow}, the weightings of the fast and slow components respectively. The average decay time is calculated using equation 2.[40]

$$\tau_{average} = \frac{A_{fast}t_{fast}^2 + A_{slow}t_{slow}^2}{A_{fast}t_{fast} + A_{slow}t_{slow}} \quad (2)$$

TDPL and polarization-based measurements were performed using a Lexel SHG 85 laser (frequency-doubled wavelength of λ = 244 nm). The PL emission signal was detected using an Andor Shamrock 303i spectrograph attached to a charge-coupled device (CCD) camera.

3. RESULTS AND DISCUSSIONS

3.1 TE and TM modes in III-nitride semiconductors

The valence band in group-III-Nitride compounds consists of degenerate states, namely, heavy-hole (HH), light-hole (LH), and crystal-field split-off (SH) states[41]. Prior studies showed that the arrangment of these energy states in the valence band of GaN, AlGaN, and AlN are noticeably different.[41] Carriers in HH bands have different angular momentum projections than those in LH bands in group III-Nitride semiconductors, which is crucial in defining the modes of carrier recombination, i.e., transverse electric (TE) and transverse magnetic (TM) modes when.[41–43] Figure 1(a) and figure 1(b) show the energy band structure of GaN and AlN respectively. These schematics show the transformation of the TE

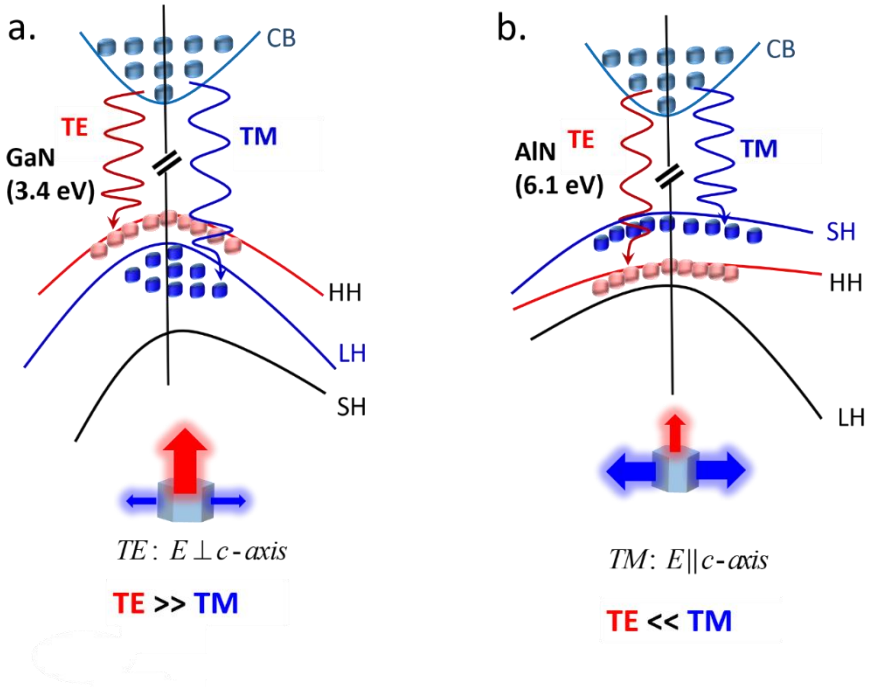

Figure 1. Energy band structure of (a) GaN, and (b) AlN near the Γ-valley where the horizontal and vertical represent the wave vector and band energy respectively. (Note the diagrams are not drawn to scale)

dominant mode to TM-dominant mode upon alloying excessive "Al" in $Al_xGa_{1-x}N$. The TE mode is suppressed when $x > 0.25$ ($\lambda < 315$ nm) for bulk $Al_xGa_{1-x}N$;[44] however, more Al can be alloyed when $Al_xGa_{1-x}N$ quantum wells (QWs) are strained to AlN barriers, i.e. valance band crossover takes place for $x > 0.57$. This shows the viability of TE-dominant UV emitters for $Al_xGa_{1-x}N$ ($x < 0.57$).[45] Nonetheless, the realization of TE-dominant deep UV emitters simply relying on "Al"-rich ($x > 0.57$) of $Al_xGa_{1-x}N$ is jeopardized.

3.2 Structural Characterization Results

Figure 2(a) is the schematic illustration of GaN QDisks embedded in the AlN NWs. The top view and side view of the AlN NWs using SEM is shown in figures 2(b) and 2 (c). It displays the NWs are dense and grown largely vertically on Si-substrate. The STEM images of 3 different samples: bulk GaN, 5-folds GaN/AlN , and 10-folds GaN/AlN are shown in figure 2(d), figure 2(e), and figure 2(f) respectively, where the AlN (GaN) are represented by dark part (bright part) respectively. The active region in all three NWs samples was expected to be 30 nm; however, the actual thickness of the

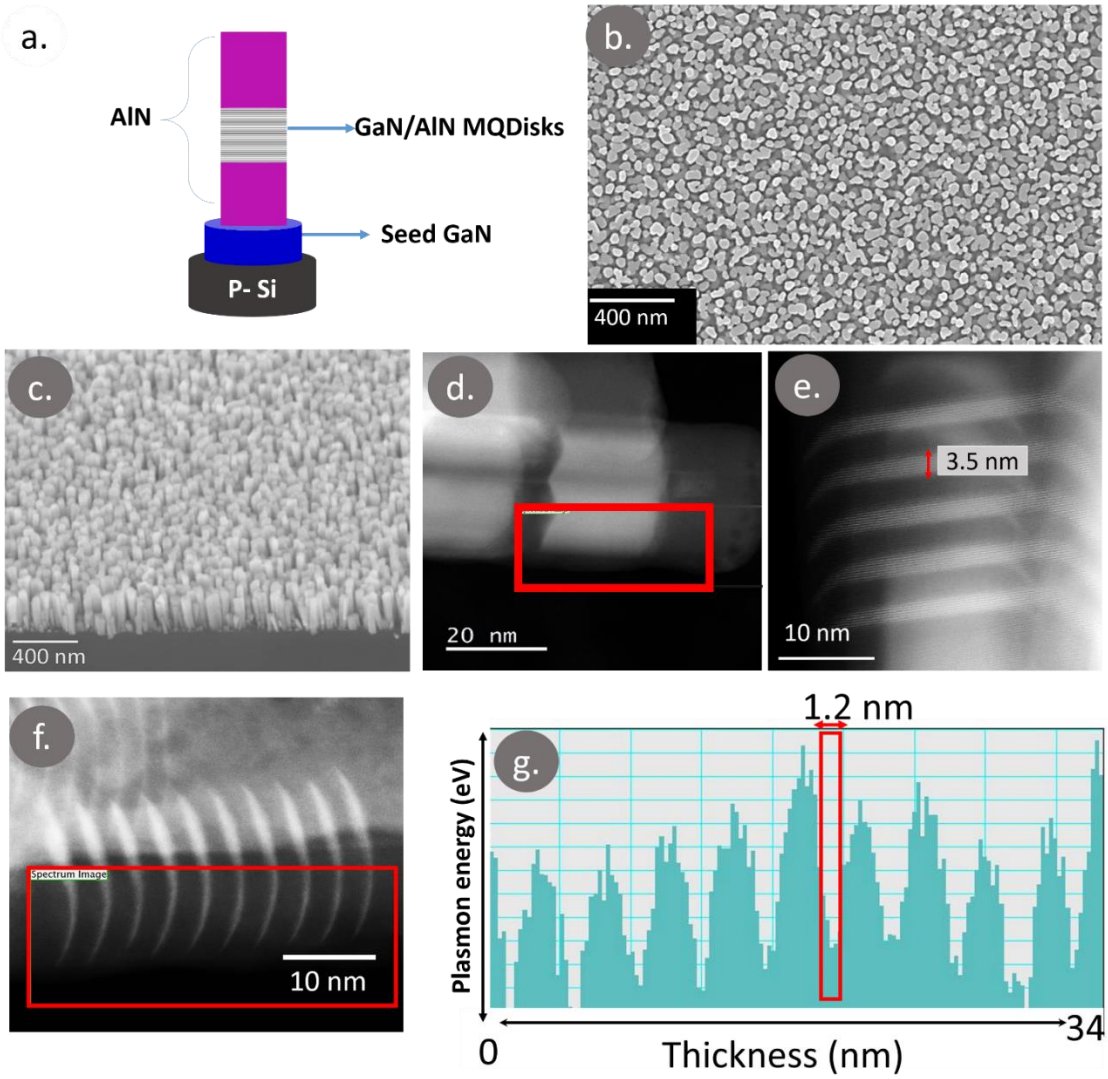

Figure 2 Schematic and images of GaN QDisks of various thicknesses confined in an AlN matrix in freely standing NWs

Figure 2. Schematic and images of GaN QDisks of various thicknesses confined in an AlN matrix in freely standing NWs grown on a Si-substrate: (a) schematic of the QDisks, (b) top view of an SEM image of NWs and, (c) tilted 45° side view. High-angle annular dark field scanning transmission electron microscopy (HAADF-STEM) of NWs illustrating (d) ~ 20 nm GaN layer, (e) thin GaN QDisks each of thickness ~ 3.5 nm, (f) ultrathin thin GaN QDisks each of thickness ~1.2 nm embedded the AlN matrix. (g) Bulk plasmon energy profile of the area marked by red rectangle in (f)

bulk GaN is found to be ~ 20 nm, using STEM. The discrepancy observed in the thickness of bulk GaN could be the effect of unforeseen temperature fluctuations during the NWs growth in the PAMBE growth chamber. For the other two samples (5-folds GaN/AlN and 10-folds GaN/AlN), the actual thickness of the active region turns out to be ~ 30 nm, as expected. The average thickness of each GaN QDisks in 5-folds GaN/AlN and 10-folds GaN/AlN obtained from the STEM images are estimated to be 3.5 nm and 1.2 nm respectively. The curvature observed in the GaN QDisks shows that the GaN QDisks embedded in AlN NWs not only grow on the c-plane (polar) but also along the semipolar axis. The details regarding the growth of GaN QDisks on various planes and the strain evolution on these QDisks has been reported earlier.[32]

3.3 Optical Characterization Results

After investigating the structural integrities using SEM and STEM, we aim to explore the optical properties of these samples. Figure 3 (a) shows the schematic diagram of the three samples under investigation. The normalized PL spectra of these samples measured at room temperature (RT) is shown in figure 3 (b). The blue shift observed in 5-folds GaN/AlN (310 nm), and 10-folds GaN/AlN (260 nm) compared to the emission observed in bulk GaN (360 nm) confirms the strong size dependent quantum confinement. The multi-peak emission observed in 10-folds GaN/AlN QDisks is attributed to the variable thickness of the QDisks grown on the different crystal planes; however it can be the effect various phenomena like crystal facet dependent emission, two-state energy transition, thickness-dependent emission not necessarily from the different facets of the same QDisks but from the cluster of QDisks, and the emission from the QDisks with variable thicknesses.[31] Since our aim is to realize efficient deep UV emission using GaN/AlN multiple QDisks structures, the further optical characterization is focused on the 10-folds GaN/AlN QDisks sample.

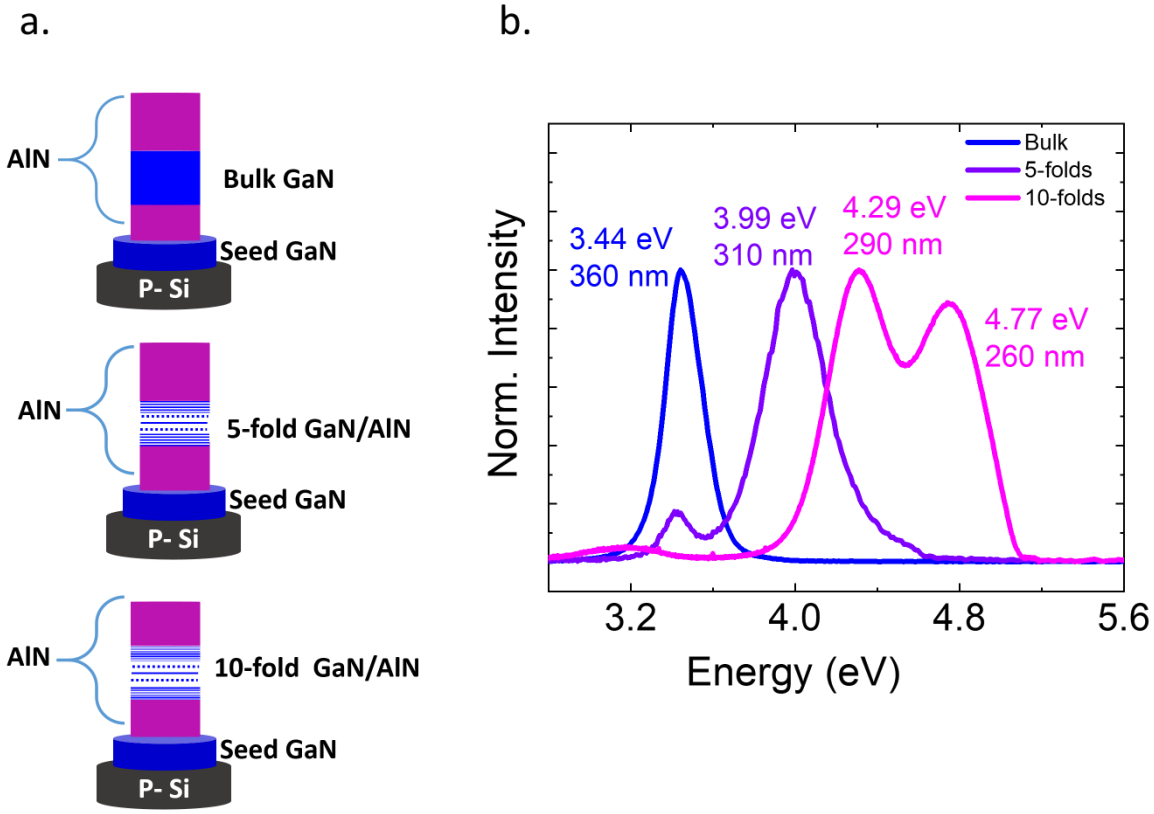

Figure 3. (a) Schematic of the GaN QDisks of various thicknesses (decreasing thickness of GaN QDisks as we go from top to bottom) confined in an AlN matrix in freely standing NWs grown on a Si-substrate, (b) Plot of normalized PL spectra of the 3 different samples measured at RT: Bulk GaN (blue), 5-folds GaN/AlN QDisks (Violet), 10-folds GaN/AlN QDisks (Pink) demonstrating the size dependent quantum confinement.

Subsequently after RT PL measurements , temperature dependent steady-state and time resolved measurements were carried out. The laser excitation power density of 1 Wcm^{-2} was chosen for the TDPL measurements and the TDPL spectra for 10-folds GaN/AlN QDisks sample is shown in figure 4(a). Interestingly, the quenching behavior of PL intensity for 2 peaks: high energy peak (260 nm) and low energy peak (290 nm) is found to be different. Generally, PL intensity quenches with increasing temperature, which is the case for the 290-nm-peak. However, the change in the PL intensity of the 260-nm-peak with respect to the changing temperature is not as significant as in 290-nm-peak and the PL intensity in

this case maximizes at 180 K unlike 290-nm-peak. This anomalous behavior of TDPL in 260-nm peak is due to the separation of holes in the LH and HH bands because light holes are assumed to be trapped in the AlN barrier at low temperature. As the temperature is slightly increased the holes get thermally activated to overcome the barrier in contributing the radiative recombination.[31] When temperature is sufficiently increased (> 180 K), PL intensity is quenched because of the regular thermalization. Figure 4(b),(i) and (ii) are the normalized IPL plots plotted against the inverse temperature in order to estimate the IQE. In an ideal condition, all of the nonradiative recombination are considered to be frozen at 4 K, i.e., IQE~1 at 4K.[31] However, it is not always guaranteed that the IQE would maximize at the lowest temperature. Nevertheless, IPL is normalized with the highest value of the IPL among all the temperatures in order to estimate the IQE. Based on the above assumption, we estimate the IQE for 290-nm-peak and 260-nm-peak to be 76% and 80 % respectively.

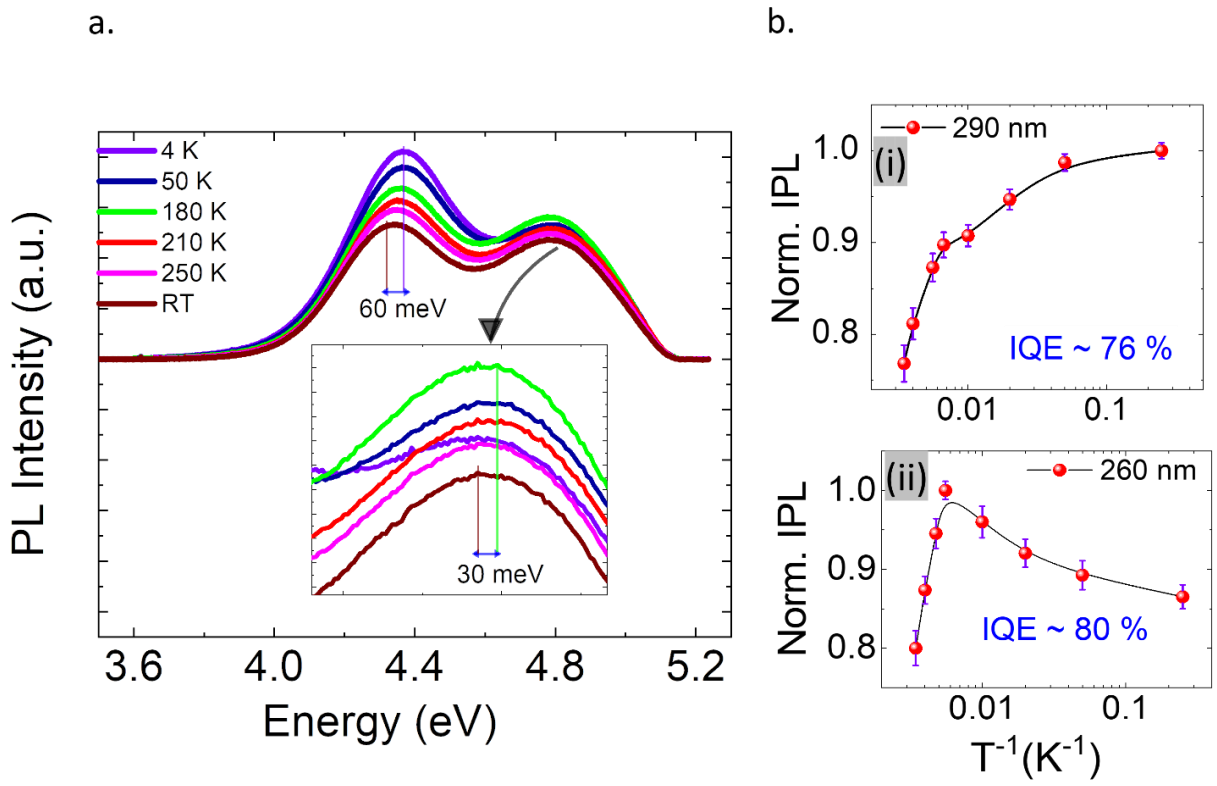

Figure 4. (a) TDPL spectra measured at different temperatures (4 K through RT), with the inset showing the zoomed section of the high-energy peak (260 nm). The temperature dependent peak shifts observed in the TDPL spectra are observed to ~ 30 meV and ~ 60 meV for 260 nm and 290 nm , respectively. (b) The Normalized IPL versus the inverse temperature for (i) 290 nm, and (ii) 260 nm.

To compliment the steady state PL measurement, we also performed temperature dependent TRPL measurements. Figure 5(a) and figure 5(b) show the decay transients of 290-nm-peak and 260-nm-peak respectively, fitted with a second order exponential decay equation. Two key parameters after the fit are the decay times: (i) fast decay time (t_{fast}) and (ii) slow decay time (t_{slow}). Commonly, t_{fast} is associated with fast thermal phenomena such as the cooling of hot carriers, photon−phonon interactions, and Coulombic interactions, which result in nonradiative recombination.[46] On the other hand, t_{slow} is taken as the total PL decay time. With the parameters t_{fast}, t_{slow}, A_{slow}, and A_{fast}, average decay time (τ_{avg}) was calculated for each peak and plotted in figure 5(c) and figure 5 (d) for 290-nm-peak and 260-nm-peak respectively for

various temperatures. The fluctuation of τ_{avg} over the temperature range of (4 K – RT) for 290-nm-peak is greater than that of 260-nm-peak, which can be correlated to the fluctuation of PL intensity in the same temperature range as discussed earlier. (see Figure 4)

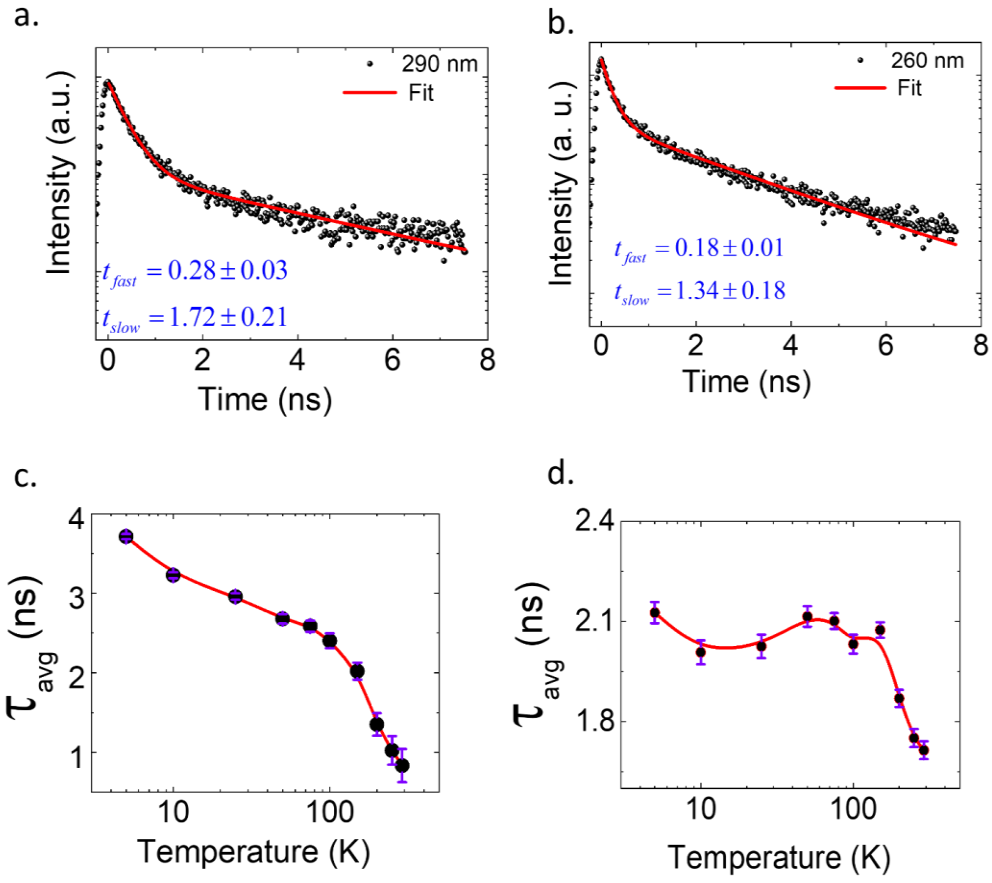

Figure 5. Sample decay transients at RT fitted using a double exponential decay for (a) 290 nm (b) 260 nm, (c) Temperature dependent average decay time for (c) 290 nm, (d) 260 nm calculated using the parameters derived from the double exponential decay fit, using equation (2)

Our final and one of the key measurements in our experiment is the investigation of the optical polarization property of GaN Qdisks. The optical polarization setup we used to examine polarization dependent measurements of PL emission of the ultrathin GaN QDisks is shown in figure 6(a). The PL emission splits into $I_{\parallel}$ (electric field parallel to the c-axis) and $I_{\perp}$ (electric field perpendicular to the c-axis) as it passes through the Glan-Taylor (G-T) polarizer. We obtain the $I_{\parallel}$ and $I_{\perp}$ components for different polarization angles ($5° \le \theta \le 60°$) as the G-T polarizer rotates about the propagation direction of light. The TE-TM components and degree of polarization (P) are assessed in terms of $I_{\parallel}$ and $I_{\perp}$ using the following equations (3-7).[30,32,47,48]

$$I_{\parallel} = I_{TEx} \tag{3}$$

$$I_{\perp} = I_{TE\,y}\cos^2\theta + I_{TM}\sin^2\theta \tag{4}$$

$$TE_{Total} = I_{TE\,y}\cos^2\theta + I_{TE\,x} \tag{5}$$

$$TM_{Total} = I_{TM}\sin^2\theta \tag{6}$$

$$P = \frac{TE\text{-}TM}{TE + TM} \tag{7}$$

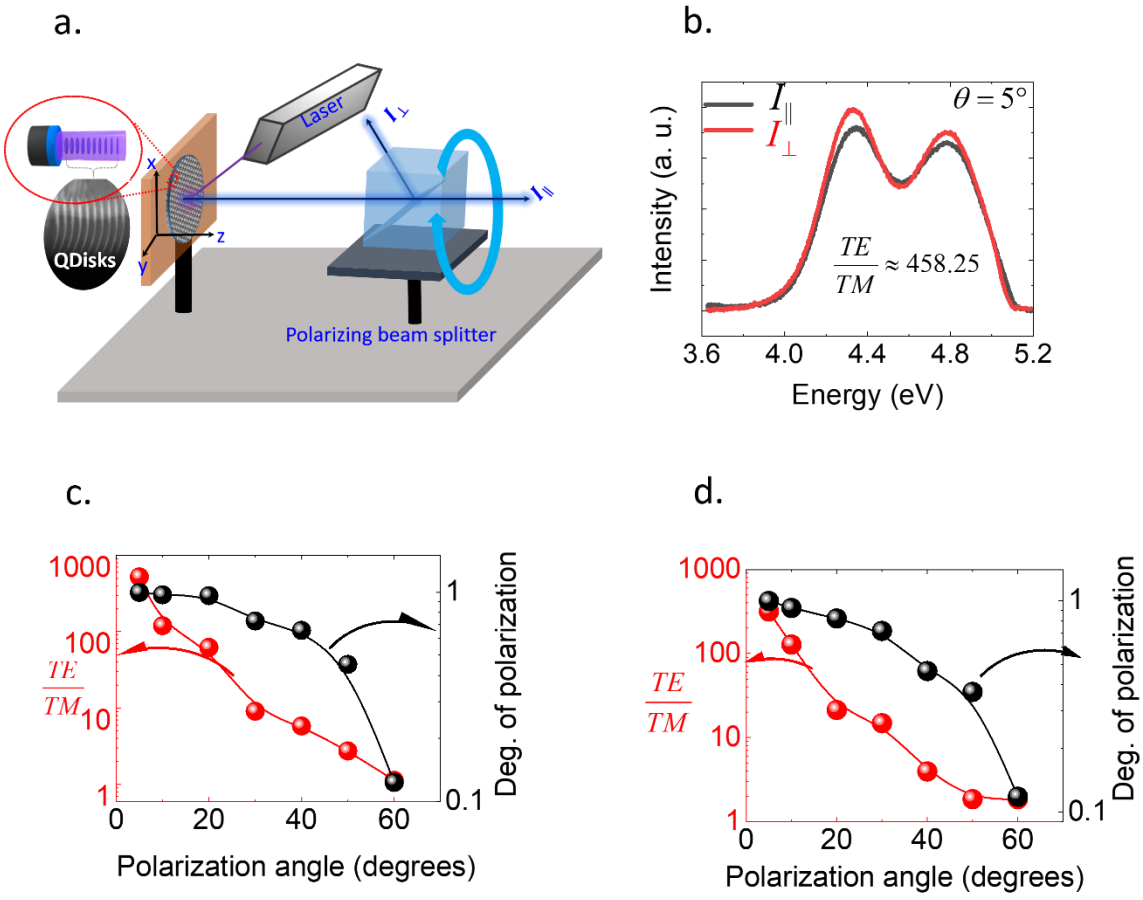

Figure 6. (a) Schematic of the experimental setup used for the optical polarization measurements, (b) Sample curve of $I_{\perp}$ (red line) and $I_{||}$ (black) at $\theta = 5°$ showing the TE/TM to be 458.25. The illustration of the ratio of TE to TM (TE/TM) and degree of polarization (P) (c) 290 nm, (d) 260 nm.

where I_{TM} is the intensity of the TM mode and I_{TEx} and I_{TEy} are the intensities of the TE mode along the x-axis and y-axis, respectively. Given the isotropic nature of the emission in the x-y plane, the values for I_{TEx} and I_{TEy} are identical.[49] The value of the polarization (P) ranges from -1 (for a pure TM mode) to 1 (for a pure TE mode); a nonzero positive value of 'P' is the sign of TE-dominant emission. Figure 6(b) illustrates the $I_{\perp}$ and $I_{||}$ measured at RT at $\theta = 5°$, where the ratio of TE to TM is found to be 458.25. Since the PL spectra consist of two peaks, it will be only fair to deconvolute each

spectrum at all the angles into two peaks and evaluate the polarization property of each peak separately. After deconvoluting each peak at different angles, the ratio of TE to TM (TE/TM), and the degree of polarization (P) were evaluated using equations (3-7). Figures 6(c) and 6(d) summarize "TE/TM", and "P" for low-energy peak (290 nm) and high-energy peak (260 nm) respectively. The pattern with which "TE/TM" and "P" change with respect to the polarization angle for the two peaks is similar even though the numerical values slightly differ. The numerical value of the "TE/TM" are different for each peak even though the value maximizes for both the cases at $\theta = 5°$. A positive value of P" indicates a TE-dominant mode:[32] it is important to note that the values of "P" are 0.116 and 0.117 for the 260 and286 nm peaks, respectively, even at θ=60°. As theoretically stated in the literatures, we experimentally confirmed the enhancement of the TE mode using ultrathin GaN QDisks in the AlN NWs matrix to realize efficient deep-UV surface emitters.

4. CONCLUSION

In conclusion, the growth, structural and optical characteristics of plasma-assisted MBE grown GaN QDisks embedded in AlN NWs were examined. Size dependent high quantum confinement of the charge carriers has been demonstrated through three different GaN QDisks samples with varying thicknesses. Temperature dependent steady-state and time resolved PL were studied to understand the internal quantum efficiency and the carrier dynamics. More importantly, angle dependent polarization dependent PL measurements were performed to realize highly efficient transverse-electric-dominant UV-C emission, thereby demonstrating the use of ultrathin GaN QDisks embedded in AlN NWs matrix can offer an excellent platform towards achieving highly efficient UV-C emitters.

5. ACKNOWLWDGEMENT

We acknowledge the financial support from the King Abdulaziz City for Science and Technology (KACST) under grant no .KACST TIC R2-FP-008. This work was partially supported by the King Abdullah University of Science and Technology(KAUST) baseline funding no. BAS/1/1614-01-01 and MBE equipment funding no. C/M-20000-12-001-77 and KCR/1/4055-01-01.

REFERENCES

[1] Priante, D., Janjua, B., Prabaswara, A., Subedi, R. C., Elafandy, R. T., Lopatin, S., Anjum, D. H., Zhao, C., Ng, T. K. and Ooi, B. S., "Ti/TaN Bilayer for Efficient Injection and Reliable AlGaN Nanowires LEDs," Conf. Lasers Electro-Optics, JTu2A.91, OSA, Washington, D.C. (2018).

[2] Kim, D. Y., Park, J. H., Lee, J. W., Hwang, S., Oh, S. J., Kim, J., Sone, C., Schubert, E. F. and Kim, J. K., "Overcoming the fundamental light-extraction efficiency limitations of deep ultraviolet light-emitting diodes by utilizing transverse-magnetic-dominant emission," Light Sci. Appl. **4**(4), e263–e263 (2015).

[3] Li, J., Fan, Z. Y., Dahal, R., Nakarmi, M. L., Lin, J. Y. and Jiang, H. X., "200nm deep ultraviolet photodetectors based on AlN," Appl. Phys. Lett. **89**(21), 213510 (2006).

[4] Kneissl, M., Seong, T.-Y., Han, J. and Amano, H., "The emergence and prospects of deep-ultraviolet light-emitting diode technologies," Nat. Photonics **13**(4), 233–244 (2019).

[5] Alias, M. S., Tangi, M., Holguin-Lerma, J. A., Stegenburgs, E., Alatawi, A. A., Ashry, I., Subedi, R. C., Priante, D., Shakfa, M. K., Ng, T. K. and Ooi, B. S., "Review of nanophotonics approaches using nanostructures and nanofabrication for III-nitrides ultraviolet-photonic devices," J. Nanophotonics **12**(04), 043508 (2018).

[6] Asif Khan, M., "AlGaN multiple quantum well based deep UV LEDs and their applications," Phys. status solidi **203**(7), 1764–1770 (2006).

[7] Khan, A., Balakrishnan, K. and Katona, T., "Ultraviolet light-emitting diodes based on group three nitrides," Nat. Photonics **2**(2), 77–84 (2008).

[8] Nakamura, S., Senoh, M. and Mukai, T., "P-gan/n-ingan/n-gan double-heterostructure blue-light-emitting diodes," Jpn. J. Appl. Phys. **32**(1 A), L8–L11 (1993).

[9] Nakamura, S., Senoh, M. and Mukai, T., "High-power InGaN/GaN double-heterostructure violet light emitting diodes," Appl. Phys. Lett. **62**(19), 2390–2392 (1993).

[10] Nakamura, S., "Current status of GaN-based solid-state lighting," MRS Bull. **34**(2), 101–107 (2009).

[11] Hsu, Y. C., Lo, I., Shih, C. H., Pang, W. Y., Hu, C. H., Wang, Y. C. and Chou, M. M. C., "InGaN/GaN single-

quantum-well microdisks," Appl. Phys. Lett. **100**(24), 242101 (2012).
[12] Bryan, I., Bryan, Z., Mita, S., Rice, A., Hussey, L., Shelton, C., Tweedie, J., Maria, J. P., Collazo, R. and Sitar, Z., "The role of surface kinetics on composition and quality of AlGaN," J. Cryst. Growth **451**, 65–71 (2016).
[13] Jones, K. A., Chow, T. P., Wraback, M., Shatalov, M., Sitar, Z., Shahedipour, F., Udwary, K. and Tompa, G. S., "AlGaN devices and growth of device structures," J. Mater. Sci. **50**(9), 3267–3307 (2015).
[14] Pelá, R. R., Caetano, C., Marques, M., Ferreira, L. G., Furthmüller, J. and Teles, L. K., "Accurate band gaps of AlGaN, InGaN, and AlInN alloys calculations based on LDA-1/2 approach," Appl. Phys. Lett. **98**(15), 151907 (2011).
[15] Hirayama, H., Maeda, N., Fujikawa, S., Toyoda, S. and Kamata, N., "Recent progress and future prospects of AlGaN-based high-efficiency deep-ultraviolet light-emitting diodes," Jpn. J. Appl. Phys. **53**(10), 100209 (2014).
[16] Zhang, J., Zhao, H. and Tansu, N., "Effect of crystal-field split-off hole and heavy-hole bands crossover on gain characteristics of high Al-content AlGaN quantum well lasers," Appl. Phys. Lett. **97**(11), 111105 (2010).
[17] Kong, W.-Y., Wu, G.-A., Wang, K.-Y., Zhang, T.-F., Zou, Y.-F., Wang, D.-D. and Luo, L.-B., "Graphene-β-Ga_2O_3 Heterojunction for Highly Sensitive Deep UV Photodetector Application," Adv. Mater. **28**(48), 10725–10731 (2016).
[18] Laleyan, D. A., Zhao, S., Woo, S. Y., Tran, H. N., Le, H. B., Szkopek, T., Guo, H., Botton, G. A. and Mi, Z., "AlN/h-BN Heterostructures for Mg Dopant-Free Deep Ultraviolet Photonics," Nano Lett. **17**(6), 3738–3743 (2017).
[19] Orita, M., Ohta, H., Hirano, M. and Hosono, H., "Deep-ultraviolet transparent conductive β-Ga2O3 thin films," Appl. Phys. Lett. **77**(25), 4166–4168 (2000).
[20] Alfaraj, N., Min, J. W., Kang, C. H., Alatawi, A. A., Priante, D., Subedi, R. C., Tangi, M., Ng, T. K. and Ooi, B. S., "Deep-ultraviolet integrated photonic and optoelectronic devices: A prospect of the hybridization of group III-nitrides, III-oxides, and two-dimensional materials," J. Semicond. **40**(12), 121801 (2019).
[21] Cui, X. Y., Delley, B. and Stampfl, C., "Band gap engineering of wurtzite and zinc-blende GaN/AlN superlattices from first principles," J. Appl. Phys. **108**(10), 103701, American Institute of PhysicsAIP (2010).
[22] Kamiya, K., Ebihara, Y., Shiraishi, K. and Kasu, M., "Structural design of AlN/GaN superlattices for deep-ultraviolet light-emitting diodes with high emission efficiency," Appl. Phys. Lett. **99**(15), 151108 (2011).
[23] Taniyasu, Y. and Kasu, M., "Polarization property of deep-ultraviolet light emission from C-plane AlN/GaN short-period superlattices," Appl. Phys. Lett. **99**(25), 251112 (2011).
[24] Bayerl, D., Islam, S., Jones, C. M., Protasenko, V., Jena, D. and Kioupakis, E., "Deep ultraviolet emission from ultra-thin GaN/AlN heterostructures," Appl. Phys. Lett. **109**(24), 241102 (2016).
[25] Sun, W., Tan, C.-K. K. and Tansu, N., "AlN/GaN Digital Alloy for Mid- and Deep-Ultraviolet Optoelectronics," Sci. Rep. **7**(1), 1–8 (2017).
[26] Selles, J., Brimont, C., Cassabois, G., Valvin, P., Guillet, T., Roland, I., Zeng, Y., Checoury, X., Boucaud, P., Mexis, M., Semond, F. and Gayral, B., "Deep-UV nitride-on-silicon microdisk lasers," Sci. Rep. **6**(1), 1–7 (2016).
[27] Shan, M., Zhang, Y., Tran, T. B., Jiang, J., Long, H., Zheng, Z., Wang, A., Guo, W., Ye, J., Chen, C., Dai, J. and Li, X., "Deep UV Laser at 249 nm Based on GaN Quantum Wells," ACS Photonics **6**(10), 2387–2391 (2019).
[28] Islam, S. M., Protasenko, V., Lee, K., Rouvimov, S., Verma, J., Xing, H. (Grace) and Jena, D., "Deep-UV emission at 219 nm from ultrathin MBE GaN/AlN quantum heterostructures," Appl. Phys. Lett. **111**(9), 091104 (2017).
[29] Wang, Y., Rong, X., Ivanov, S., Jmerik, V., Chen, Z., Wang, H., Wang, T., Wang, P., Jin, P., Chen, Y., Kozlovsky, V., Sviridov, D., Zverev, M., Zhdanova, E., Gamov, N., Studenov, V., Miyake, H., Li, H., Guo, S., et al., "Deep Ultraviolet Light Source from Ultrathin GaN/AlN MQW Structures with Output Power Over 2 Watt," Adv. Opt. Mater. **7**(10), 1801763 (2019).
[30] Liu, C., Ooi, Y. K., Islam, S. M., Verma, J., Xing, H. (Grace), Jena, D. and Zhang, J., "Physics and polarization characteristics of 298 nm AlN-delta-GaN quantum well ultraviolet light-emitting diodes," Appl. Phys. Lett. **110**(7), 071103 (2017).
[31] Sarwar, A. T. M. G., May, B. J., Chisholm, M. F., Duscher, G. J., Myers, R. C., Golam Sarwar, A. T. M., May, B. J., Chisholm, M. F., Duscher, G. J. and Myers, R. C., "Ultrathin GaN quantum disk nanowire LEDs with sub-250 nm electroluminescence," Nanoscale **8**(15), 8024–8032 (2016).
[32] Subedi, R. C., Min, J. W., Mitra, S., Li, K. H., Ajia, I., Stegenburgs, E., Anjum, D. H., Conroy, M., Moore, K., Bangert, U., Roqan, I. S., Ng, T. K. and Ooi, B. S., "Quantifying the Transverse-Electric-Dominant 260 nm Emission from Molecular Beam Epitaxy-Grown GaN-Quantum-Disks Embedded in AlN Nanowires: A

Comprehensive Optical and Morphological Characterization," ACS Appl. Mater. Interfaces **12**(37), 41649–41658 (2020).
[33] Zhao, C., Alfaraj, N., Chandra Subedi, R., Liang, J. W., Alatawi, A. A., Alhamoud, A. A., Ebaid, M., Alias, M. S., Ng, T. K. and Ooi, B. S., "III-nitride nanowires on unconventional substrates: From materials to optoelectronic device applications," Prog. Quantum Electron. **61**, 1–31 (2018).
[34] Pan, H. and Feng, Y. P., "Semiconductor Nanowires and Nanotubes: Effects of Size and Surface-to-Volume Ratio," ACS Nano **2**(11), 2410–2414 (2008).
[35] Glotzer, S. C., "Shape matters," Nature **481**(7382), 450–452 (2012).
[36] Yan, R., Gargas, D. and Yang, P., "Nanowire photonics," Nat. Photonics **3**(10), 569–576 (2009).
[37] Guo, W., Zhang, M., Banerjee, A. and Bhattacharya, P., "Catalyst-Free InGaN/GaN Nanowire Light Emitting Diodes Grown on (001) Silicon by Molecular Beam Epitaxy," Nano Lett. **10**(9), 3355–3359 (2010).
[38] Priante, D., Janjua, B., Prabaswara, A., Subedi, R. C., Elafandy, R. T., Lopatin, S., Anjum, D. H., Zhao, C., Ng, T. K. and Ooi, B. S., "Highly uniform ultraviolet-A quantum-confined AlGaN nanowire LEDs on metal/silicon with a TaN interlayer," Opt. Mater. Express **7**(12), 4214 (2017).
[39] Tangi, M., Min, J.-W. W., Priante, D., Subedi, R. C., Anjum, D. H., Prabaswara, A., Alfaraj, N., Liang, J. W., Shakfa, M. K., Ng, T. K. and Ooi, B. S., "Observation of piezotronic and piezo-phototronic effects in n-InGaN nanowires/Ti grown by molecular beam epitaxy," Nano Energy **54**, 264–271 (2018).
[40] Xin, B., Pak, Y., Mitra, S., Almalawi, D., Alwadai, N., Zhang, Y. and Roqan, I. S., "Self-Patterned CsPbBr 3 Nanocrystals for High-Performance Optoelectronics," ACS Appl. Mater. Interfaces **11**(5), 5223–5231 (2019).
[41] Jmerik, V. N., Nechaev, D. V. and Ivanov, S. V., "Kinetics of Metal-Rich PA Molecular Beam Epitaxy of AlGaN Heterostructures for Mid-UV Photonics," [Molecular Beam Epitaxy], Elsevier, 135–179 (2018).
[42] Suzuki, M. and Uenoyama, T., "Strain effect on electronic and optical properties of GaN/AlGaN quantum-well lasers," J. Appl. Phys. **80**(12), 6868–6874 (1996).
[43] Ilegems, M., "III–V Compound Semiconductor Epitaxy for Optoelectronic Integration," [Optoelectronic Integration: Physics, Technology and Applications], Springer, 61–106 (1994).
[44] Nam, K. B., Li, J., Nakarmi, M. L., Lin, J. Y. and Jiang, H. X., "Unique optical properties of AlGaN alloys and related ultraviolet emitters," Appl. Phys. Lett. **84**(25), 5264–5266 (2004).
[45] Zhang, J., Zhao, H. and Tansu, N., "Effect of crystal-field split-off hole and heavy-hole bands crossover on gain characteristics of high Al-content AlGaN quantum well lasers," Appl. Phys. Lett. **97**(11), 111105 (2010).
[46] Shah, J., [Ultrafast spectroscopy of semiconductors and semiconductor nanostructures, 2nd ed.], Springer Berlin Heidelberg, Newyork (1999).
[47] Chen, X., Ji, C., Xiang, Y., Kang, X., Shen, B. and Yu, T., "Angular distribution of polarized light and its effect on light extraction efficiency in AlGaN deep-ultraviolet light-emitting diodes," Opt. Express **24**(10), A935 (2016).
[48] Shakya, J., Knabe, K., Kim, K. H., Li, J., Lin, J. Y. and Jiang, H. X., "Polarization of III-nitride blue and ultraviolet light-emitting diodes," Appl. Phys. Lett. **86**(9), 091107 (2005).
[49] Bardoux, R., Guillet, T., Gil, B., Lefebvre, P., Bretagnon, T., Taliercio, T., Rousset, S. and Semond, F., "Polarized emission from GaN/AlN quantum dots: Single-dot spectroscopy and symmetry-based theory," Phys. Rev. B - Condens. Matter Mater. Phys. **77**(23), 235315 (2008).